

# Numerical research on cross-ventilation flow of a generic building in unsheltered and sheltered conditions: impact of cross-section

Puxian Ding<sup>1,2,3\*</sup>, Xiaoqing Zhou<sup>1,2,3</sup>, Weihao Chen<sup>1,2,3</sup>, and Wuduo Jin<sup>1,2,3</sup>

<sup>1</sup>Academy of Building Energy Efficiency of Guangzhou University, 510006 Guangzhou, China

<sup>2</sup>Guangdong Provincial Key Laboratory of Building Energy Efficiency and Application Technologies, 510006 Guangzhou, China

<sup>3</sup>School of Civil Engineering, Guangzhou University, 510006 Guangzhou, China

**Abstract.** The performances of ventilation in the buildings with quadrate and cylindrical cross-sections are compared numerically. The incoming jet in the cylindrical unsheltered-building is more horizontal in comparison to the quadrate unsheltered-building. The dimensionless volume flow rates in the quadrate and cylindrical unsheltered-buildings are respectively 0.503 and 0.553. The incoming jet in the sheltered-buildings flows to the floors immediately. The velocity near the floor in the cylindrical sheltered-building is greater than that in the quadrate sheltered-building. The dimensionless volume flow rates in the quadrate and cylindrical sheltered-buildings are respectively 0.130 and 0.210. Comparing with the quadrate buildings, the ventilation rates in the cylindrical unsheltered and sheltered buildings increased by 10% and 61%.

## 1 Introduction

Cross-ventilation driven by wind pressure difference is an important ventilation method since it can provide a fast and effective way to remove large amounts of pollutants and internal heat from a building [1-2]. This is good for air-quality improvement and building energy reduction. The rate of the ventilation is the key factor in designing the cross-ventilation [3-4]. The ventilation rate of a building depends on the size and the position of the windows, the building roof and the airflow conditions around the building and so on [5-7]. The cross-section of the buildings influences the airflow around buildings significantly. However, the effects of the cross-section of the buildings on the cross-ventilation are rarely studied. In this paper, numerical study on the cross-ventilation flow of a generic cylindrical building in unsheltered and sheltered conditions is conducted.

An efficient hybrid turbulence numerical method based on the production-limited eddy simulation (PLES) proposed by us in the previous paper [8] is applied. The buildings are located within the atmospheric boundary layer.

## 2 Description of study cases

For analysing the cross-ventilation flow of a generic cylindrical building in unsheltered and sheltered conditions shown in Figs. 1 and 2, the results of the wind tunnel experiments conducted by Tominaga and Blocken [9] and Shirzadi et al. [10] are chosen as the referred for validation. Two conditions including a generic building unsheltered and sheltered shown in Fig.

1 are considered. The sheltered condition is the situation that the target building is surrounded with eight similar buildings without opening, which are arranged in a regular configuration with a planar area ratio of 0.25 displayed in Fig.1-(b). The wind speed at the unsheltered and the sheltered buildings' height were measured to be 4.3m/s [9] and 5.2m/s [10], yielding Reynolds numbers about 45 000 and 54 000.

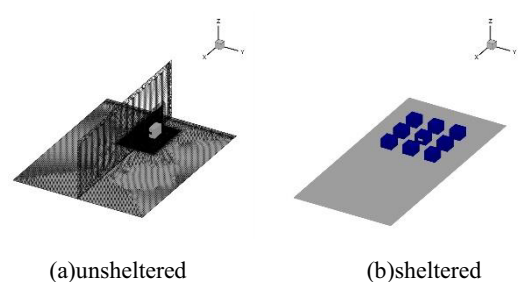


**Fig. 1.** Computational domain of the cases of quadrate building.

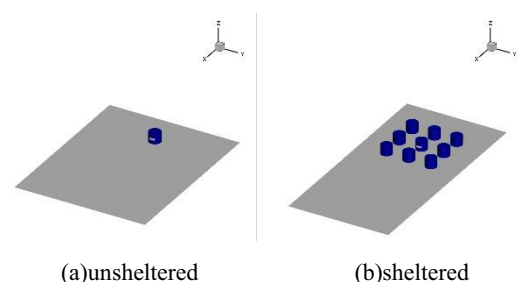


**Fig. 2.** Computational domain of the cases of cylindrical building.

## 3 Simulation method

Corresponding author: [tingalan@foxmail.com](mailto:tingalan@foxmail.com)

The air is incompressible and Newtonian fluid. The continuity and momentum governing equations can be written in the Cartesian tensor form as follows.

$$\frac{\partial \rho}{\partial t} + \frac{\partial}{\partial x_i}(\rho \bar{u}_i) \quad (1)$$

$$\frac{\partial}{\partial t}(\rho \bar{u}_i) + \frac{\partial}{\partial x_j}(\rho \bar{u}_i \bar{u}_j) = -\frac{\partial \bar{p}}{\partial x_i} + \frac{\partial}{\partial x_j} \left[ \mu \left( \frac{\partial \bar{u}_i}{\partial x_j} + \frac{\partial \bar{u}_j}{\partial x_i} - \frac{2}{3} \delta_{ij} \frac{\partial \bar{u}_l}{\partial x_l} \right) \right] + \frac{\partial \tau_{ij}}{\partial x_j} \quad (2)$$

where  $u_i$  and  $u_j$  are the velocity components,  $\rho$  and  $p$  are the density and the pressure respectively,  $\mu$  is the dynamic viscosity, and  $\tau_{ij}$  represents the Reynolds stresses  $-\rho \bar{u}_i' u_j'$ . The overbar means ensemble-averaged.

The underlying RANS model of the PLES model is the SST  $k$ - $\omega$  model [11], which works as the original  $k$ - $\omega$  model within the inner boundary layer and the standard  $k$ - $\varepsilon$  model in the outer region. The modelled transport equations of the turbulence kinetic energy  $k$  and the specific dissipation rate  $\omega$  are as follows.

$$\frac{\partial}{\partial t}(\rho k) + \frac{\partial}{\partial x_i}(\rho \bar{u}_i k) = P_k - \rho \beta^* k \omega + \frac{\partial}{\partial x_i} \left[ \left( \mu + \frac{\mu_t}{\sigma_k} \right) \frac{\partial k}{\partial x_i} \right] \quad (3)$$

$$\begin{aligned} \frac{\partial}{\partial t}(\rho \omega) + \frac{\partial}{\partial x_i}(\rho \bar{u}_i \omega) &= \alpha \frac{\omega}{k} P_k - \rho \beta \omega^2 + \\ \frac{\partial}{\partial x_i} \left[ \left( \mu + \frac{\mu_t}{\sigma_\omega} \right) \frac{\partial \omega}{\partial x_i} \right] &+ 2(1-F) \frac{\rho}{\sigma_\omega \omega} \frac{\partial k}{\partial x_i} \frac{\partial \omega}{\partial x_i} \end{aligned} \quad (4)$$

The production term  $P_k$  is calculated as below.

$$P_k = \mu_t S^2, \quad S = \sqrt{2 S_{ij} S_{ij}}, \quad S_{ij} = 0.5 \left( \frac{\partial \bar{u}_i}{\partial x_j} + \frac{\partial \bar{u}_j}{\partial x_i} \right) \quad (5)$$

The turbulent viscosity  $\mu_t$  has the formula as follows.

$$\mu_t = \rho \frac{k}{\omega} \frac{1}{\max[1/\alpha, S F_2 / (0.31\omega)]} \quad (6)$$

The blending function  $F_1$  and  $F_2$ , turbulent Prandtl numbers  $\sigma_k$ ,  $\sigma_\omega$ , and model constants  $\alpha$ ,  $\beta$  are the same as those in the Ref. [11].

### 3.1 PLES model

In the PLES model, the production term of the  $k$  equation is substituted by the below formula.

$$P_{ples} = f_d P_k + (1.0 - f_d) \mu_{sgs} S^2 = f_d P_k + (1.0 - f_d) \frac{\mu_{sgs}}{\mu_t} P_k \quad (7)$$

where the shielding function  $f_d$  is shown as follows.

$$\begin{aligned} r_1 &= 0.25 - d_w / h_{\max} \\ f_{d1} &= \min \{ 2 \exp(-9r_1^2), 1.0 \} \\ r_2 &= \frac{k / \omega}{\kappa^2 d_w^2 \sqrt{0.5(S^2 + \Omega^2)}} \\ f_{d2} &= \tanh((C_{d1} r_2)^{C_{d2}}) \\ f_d &= \max(f_{d1}, f_{d2}) \end{aligned} \quad (8)$$

where  $\Omega$ ,  $d_w$ , and  $h_{\max}$  are the vorticity magnitude, the distance to the nearest wall, and the maximum edge length of the cell, respectively. The constants  $C_{d1}$  and  $C_{d2}$  respectively have the values of 20.0 and 3.0, and  $\kappa$  is the von Kármán constant having the value of 0.41. The model works as RANS mode when the shielding function  $f_d = 1.0$ , otherwise as LES mode.

The wall-adapting local eddy-viscosity (WALE) model [12] is applied as the SGS eddy viscosity in the PLES model. The WALE turbulent viscosity is calculated by the equations (10-12).

$$\mu_{sgs} = \rho L_s^2 \frac{(S_{ij}^d S_{ij}^d)^{3/2}}{(S_{ij}^d S_{ij}^d)^{5/2} + (S_{ij}^d S_{ij}^d)^{5/4}} \quad (9)$$

$$L_s = 0.325 V^{1/3} \quad (10)$$

$$S_{ij}^d = 0.5(g_{ij}^2 + g_{ji}^2) - (1/3)\delta_{ij}g_{kk}^2, \quad g_{ij} = \frac{\partial \bar{u}_i}{\partial x_j} \quad (11)$$

where  $V$  is the cell volume.

### 3.2 Boundary conditions

The velocity and turbulent kinetic energy of the inlet boundary condition are the same as the wind tunnel experiments. The turbulence dissipation rate  $\varepsilon$  and the specific dissipation rate  $\omega$  are calculated by below equations.

$$\varepsilon = C_\mu^{1/2} k \frac{d\langle u \rangle}{dz} \quad (12)$$

$$\omega = \frac{\varepsilon}{C_\mu k} = \frac{\varepsilon}{0.09k} \quad (13)$$

The symmetry boundary condition is set at the lateral and upper walls. The outflow boundary condition is used at the outlet. The building and ground surfaces are set to the wall boundary condition. The random 2D vortexes are generated on the plane away  $x/b=0.5$  ( $b$  is the length of the side wall) from the inlet where modelled turbulence kinetic energy is converted into resolved energy using the vortex method [13].

### 4 Model validation

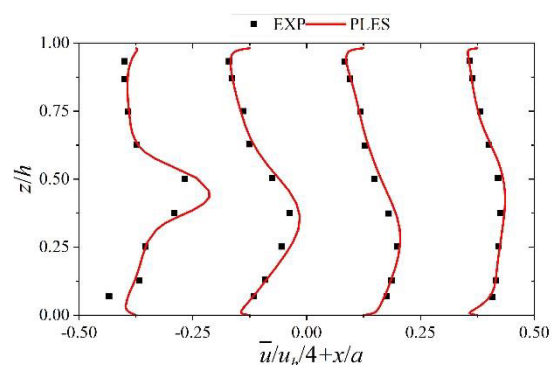


**Fig. 3.** Comparison of the mean streamwise velocity from the PLES model with the experimental result in the unsheltered condition.

The comparisons of mean streamwise velocity from the PLES model with the experimental results in the unsheltered and the sheltered conditions are shown in Figs. 3 and 4 respectively. These profiles prove that the PLES model can obtain satisfactory simulation results. Taken the experimental results from the reported papers as the basic data, the errors of the volume ventilation rates in the unsheltered and sheltered cases are

respectively 0.6% and 8.3%. The normalized mean square errors of the time-averaged streamwise velocity are respectively 0.002 and 0.005. The comparisons of the simulation results with the experimental data show that the utilized numerical method is capable of predicting the cross-ventilation flow of a generic building in unsheltered and sheltered conditions.

## 5 Results and discussion

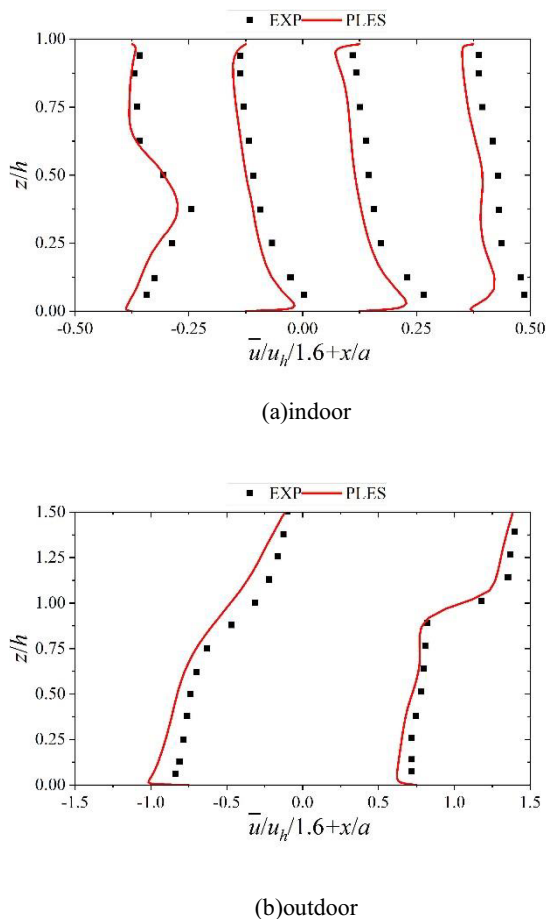


**Fig. 4.** Comparison of mean streamwise velocity from the PLES model with the experimental result in the sheltered condition.

Then, the performances of ventilation in the buildings with quadrate and cylindrical cross-sections are compared numerically. Figs. 5 and 6 give the profiles of the mean streamwise velocity for the quadrate and cylindrical unsheltered-buildings and sheltered-buildings respectively. The incoming jet in the centre of the cylindrical unsheltered-building is more horizontal in comparison to the quadrate unsheltered-building. And the mean streamwise velocity is greater in the center of the cylindrical unsheltered-building, but smaller over the floor. The dimensionless volume flow rates in the quadrate and cylindrical unsheltered-buildings are respectively 0.503 and 0.553.

The incoming jets in the sheltered-buildings flow to the floors immediately. The velocity near the floor in the

cylindrical sheltered-building is greater than that in the quadrate sheltered-building. The dimensionless volume flow rates in the quadrate and cylindrical sheltered-buildings are respectively 0.130 and 0.210.

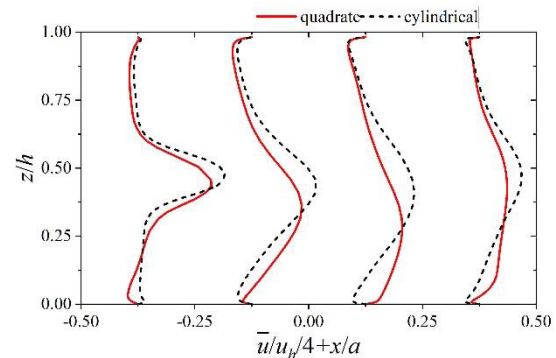


**Fig. 5.** Profiles of the mean streamwise velocity for the quadrate and cylindrical unsheltered-buildings.

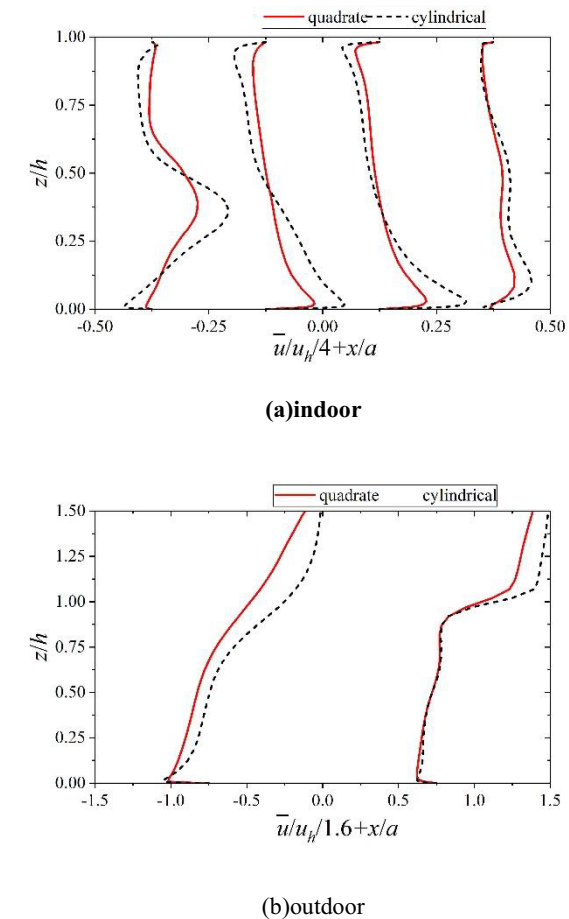


**Fig. 6.** Profiles of the mean streamwise velocity for the quadrate and cylindrical sheltered-buildings.

In summary, comparing with the quadrate buildings, the ventilation rates in the cylindrical unsheltered and sheltered buildings increased by 10% and 61%.

## 6 Conclusions

The performances of ventilation in the buildings with quadrate and cylindrical cross-sections are compared numerically. The incoming jet in the cylindrical unsheltered-building is more horizontal in comparison to the quadrate unsheltered-building. The mean streamwise velocity is greater in the center of the cylindrical unsheltered-building. The dimensionless volume flow rates in the quadrate and cylindrical unsheltered-buildings are respectively 0.503 and 0.553.

The incoming jet in the sheltered-buildings flows to the floors immediately. The velocity near the floor in the cylindrical sheltered-building is greater than that in the quadrate sheltered-building. The dimensionless volume flow rates in the quadrate and cylindrical sheltered-buildings are respectively 0.130 and 0.210.

Comparing with the quadrate buildings, the ventilation rates in the cylindrical unsheltered and sheltered buildings increased by 10% and 61%.

This work is supported by the National Natural Science Foundation of China (Grant No. 52078146), the Postdoctoral Research Project of Guangzhou (Grant No. 62104340), and the Key Project of Basic Research and Applied Basic Research in Universities of Guangdong Province (Grant No. 2018KZDXM050). We also acknowledge the Network Center of Guangzhou University for providing HPC computing resources.

## References

1. X. Zhang, A. U. Weerasuriya, J. Wang, C. Y. Li, Z.Chen, K. T. Tse , J. Hang, *Buid. Environ.*, **207**, 108447(2022).
2. F. Bazdidi-Tehrani, S. Masoumi-Verki, P. Gholamalipour, M. Kiamansouri, *Build. Simul.* **12**, 921–941 (2019).
3. N. Ikegaya, S. Hasegawa, A. Hagishima - *Buid. Environ.*, **147**, 132-145 (2019)
4. K. Kosutova, T. van Hooff, C. Vanderwel, B. Blocken, J. Hensen, *Buid. Environ.*, **154**, 263-280(2019).
5. F. Bazdidi-Tehrani, S. Masoumi-Verki, P. Gholamalipour, *Sustain. Cities Soc.*, **61**, 102196(2020).
6. Y. Tominaga, B. Blocken, *J. Wind Eng. Ind. Aerod.*, **155**, 74-88(2016).
7. H. Montazeri, F. Montazeri, *Renew. Energ.*, **118**, 502-520(2018).
8. P. Ding, X. Zhou, H. Wu, Q. Chen, *Buid. Environ.*, **210**, 108709 (2021).
9. Y. Tominaga, B. Blocken, *Buid. Environ.*, **92**, 452-461(2015)
10. M. Shirzadi, Y.Tominaga, P. A. Mirzaei, *Buid. Environ.*, **158**, 60-72(2019).
11. F. R. Menter, *AIAA J.*, **32**, 1598-1605(1994).
12. F. Nicoud, F.Ducros, *Flow Turbul. Combust.*, **62**, 183-200(1999).
13. F. Mathey, D. Cokljat, J. P. Bertoglio, E. Sergent, *Prog. Comput. Fluid Dy.*, **6**, 58-67(2006).